

MOST photometry and DDO spectroscopy of the eclipsing (white dwarf + red dwarf) binary V471 Tau¹

Krzysztof Z. Kamiński

*Astronomical Observatory, Adam Mickiewicz University
ul. Słoneczna 36, 60-286 Poznań, Poland*

chrisk@amu.edu.pl

Slavek M. Ruciński

*David Dunlap Observatory, University of Toronto
P.O. Box 360, Richmond Hill, Ontario, L4C 4Y6, Canada*

rucinski@astro.utoronto.ca

Jaymie M. Matthews, Rainer Kuschnig, Jason F. Rowe

*Department of Physics & Astronomy, University of British Columbia
6224 Agricultural Road, Vancouver, B.C., V6T 1Z1, Canada*

(matthews,kuschnig,rowe)@astro.ubc.ca

David B. Guenther

*Institute for Computational Astrophysics, Department of Astronomy and Physics,
Saint Marys University, Halifax, N.S., B3H 3C3, Canada*

guenther@crux.stmarys.ca

Anthony F. J. Moffat

*Département de Physique, Université de Montréal
C.P.6128, Succursale: Centre-Ville, Montréal
QC, H3C 3J7, Observatoire du Mont Mégantic, Canada*

moffat@astro.umontreal.ca

Dimitar Sasselov

*Harvard-Smithsonian Center for Astrophysics
60 Garden Street, Cambridge, MA 02138*

sasselov@cfa.harvard.edu

Gordon A. H. Walker

1234 Hewlett Place, Victoria, BC V8S 4P7, Canada

Department of Physics & Astronomy, University of British Columbia

6224 Agricultural Road, Vancouver, B.C., V6T 1Z1, Canada

`gordonwa@uvic.ca`

and

Werner W. Weiss

Institut für Astronomie, Universität Wien

Türkenschanzstrasse 17, A-1180 Wien, Austria

`weiss@astro.univie.ac.at`

ABSTRACT

The Hyades K2V+WD system 471 Tau is a prototype post-common envelope system and a likely cataclysmic binary progenitor. We present 10 days of nearly continuous optical photometry by the MOST (Microvariability & Oscillations of STars) satellite and partly simultaneous optical spectroscopy from DDO (David Dunlap Observatory) of the binary. The photometric data indicate that the spot coverage of the K dwarf component was less than observed in the past, suggesting that we monitored the star close to a minimum in its activity cycle. Despite the low spot activity, we still detected seven flare-like events whose estimated energies are among the highest ever observed in V471 Tau and whose times of occurrence do not correlate with the binary orbital phase. A detailed $O - C$ analysis of the times of eclipse over the last ~ 35 years reveals timing variations which could be explained in several ways, including perturbations by an as-yet-undetected third body in the system or by a small orbital eccentricity inducing slow apsidal motion. The DDO spectra result in improved determinations of the K dwarf projected rotation velocity, $V_K \sin i = 92 \text{ km s}^{-1}$, and the orbital amplitude, $K_K = 150.5 \text{ km s}^{-1}$. The spectra also allow us to measure changes in $H\alpha$ emission strength and radial velocity (RV) variations. We measure a larger $H\alpha$ velocity amplitude than found previously suggesting that the source of the emission in V471 Tau was less concentrated around the sub-white-dwarf point on the K star than had been observed in previous studies.

Subject headings: stars: close binaries – stars: eclipsing binaries – stars: variable stars – photometry: space based

1. INTRODUCTION

V471 Tau is a close eclipsing binary star ($V \sim 9$) consisting of a hot white dwarf and a red dwarf with an orbital period of 0.521 d. It is a member of the Hyades cluster (Werner & Rauch 1997) and – very likely – a cataclysmic binary progenitor (Still & Hussain 2003). V471 Tau has been the subject of numerous investigations over the past 35 years; cf. the main contributions by Skillman & Patterson (1988), Clemens et al. (1992), O’Brien et al. (2001), Ibanoglu et al. (2005) and Hussain et al. (2006).

The V471 Tau system may be the prototype of a post-common envelope binary with a white dwarf and a main sequence star. The mass and radius of both components can be measured with high accuracy, while the K dwarf which is spun up to high rotation rates by tidal forces may be an analogue for rapidly rotating pre-ZAMS stars like AB Dor. Simultaneous precise time-resolved photometry and spectroscopy which cover phases of eclipse in the V471 Tau system can sample the spot coverage of the K dwarf. Eclipse timing can measure apsidal motion in the binary and test whether the system is actually a triple one with a third undetected component. We therefore organized a coordinated campaign of spacebased photometry from the MOST satellite and groundbased spectroscopy from DDO.

We present new MOST and DDO observations of V471 Tau in Section 2. The MOST light curve and its changes are discussed in Section 3 while Section 4 gives a description of the spectroscopic observations. Section 5 summarizes the combined results.

¹Based on data from the MOST satellite, a Canadian Space Agency mission jointly operated by Dynacon Inc., the University of Toronto Institute for Aerospace Studies and the University of British Columbia, with the assistance of the University of Vienna, and on data obtained at the David Dunlap Observatory, University of Toronto.

2. OBSERVATIONS OF V471 TAU

2.1. MOST photometry

The MOST (Microvariability & Oscillations of STars) space mission (Walker et al. 2003; Matthews et al. 2004) was designed to perform high-precision optical photometry of bright stars with long time coverage and high duty cycle. MOST is equipped with a 15-cm telescope and a custom broadband filter (spectral transmission peak $\sim 5500 \text{ \AA}$ and FWHM $\sim 3000 \text{ \AA}$). The polar Sun-synchronous orbit of the satellite allows it to monitor stars in the anti-solar direction for up to 60 days without interruption.

MOST observed V471 Tau for 10.0 days during 4 – 14 December 2005 (in Terrestrial Time Julian Days: 2,453,708.5117 – 2,453,718.5122, see below in Section 3.2), covering just over 19 orbital periods of the binary system. The photometry was obtained in MOST’s Direct Imaging mode (Rowe et al. 2006), with a slightly defocused stellar image sampled in a CCD sub-raster. The exposure time was 6.52 s, sampled at 10-s intervals. Two reference stars in the same field (GSC 01252-00692, $V = 8.9$ and GSC 01252-00046, $V = 9.8$) were observed simultaneously in the same way to calibrate instrumental or satellite orbital artifacts.

The MOST instrument focal plane can be illuminated by scattered Earth light whose level is modulated by the MOST orbital period of $P_M \simeq 101$ min. The amplitude and complexity of the stray light background variations depend on the season of observing, the location of the target star relative to the bright limb of the Earth and the orientation (roll) of the spacecraft. In the case of the V471 Tau photometry, the periodic fluctuations in background translated into photometric uncertainties in the stellar signal ranging from point-to-point scatter with $\sigma \simeq 0.003$ (about 3 mmag) at stray light minimum to a point-to-point scatter of about $\sigma \geq 0.1$ at stray light maximum.

The dark and flat field corrections were performed by monitoring individual pixel responses during test exposures on fields empty of stars bright enough to rise above the background. Photometry was extracted from the stellar images using a Moffat-profile point spread function model (Moffat 1969). The correlation in the raw photometry between the instrumental magnitude light curve and the estimated sky background was removed as described in Rowe et al. (2006). About 29% of the total number of data points were rejected because of pixel saturation during phases of the highest stray light in the MOST orbit and high cosmic ray fluxes when MOST passed through the South Atlantic Anomaly, as indicated by the orbital model of the local magnetic field strength. Additionally, about 6% of data points were rejected because of the relative uncertainty exceeding $\sigma = 0.015$ of the mean light level.

The reduction and selection procedure left 56,383 measurements containing gaps of variable length spaced roughly by the MOST orbital period, resulting in a net duty cycle of about 65%. (We later conducted a period search after an even stricter selection of the data, with a duty cycle of 59%, as described in Section 3.3.) The time sampling and duty cycle provide excellent coverage in binary orbital phase and during the eclipses of V471 Tau. Note that the orbital period of the binary of close to 1/2 day always created a phase-coverage problem for ground based observations; the MOST data are entirely free of this limitation. The MOST photometry data (raw, and the reduced light curve used for analysis in this paper) are available in the MOST Public Data Archive on the Science page of the MOST web site: www.astro.ubc.ca/MOST.

2.2. V471 Tau light curve

The 19 orbital cycles of the binary monitored by MOST allowed us to investigate changes in the light curve from cycle to cycle, which is normally interpreted as migration and evolution of spots on the magnetically active K dwarf component (Ibanoglu 1978). The MOST data were divided into 1-day long subsets and those subsets were phased with the known orbital period of V471 Tau. Three of these subsets, from the beginning, middle and end of the 10-day run, are overplotted in Figure 1. A subtle trend is visible in that the rising portion of the light curve (in the phase interval 0.05 – 0.25) moves systematically later in phase with time, by a total of about 0.04 over 10 days. There is some evidence of this shift during the falling portion of the curve in the phase interval 0.75 – 0.95, but it is less pronounced. No phase shift is seen in the phase range 0.3 – 0.7, within the photometric scatter.

The changes seen in the MOST photometry resemble the “photometric wave migration” first reported by Ibanoglu (1978) and discussed below in Section 3.1. The average shift of the wave of ~ 0.002 phase/day indicates that it would take 500 ± 250 days for the wave to make a full revolution (P_{migr}). This is somewhat longer than the wave migration period found in previous studies (from ~ 180 d by Ibanoglu (1989) to 372 d by Skillman & Patterson (1988)), although our estimate of the drift rate, based on only 19 orbital cycles, is necessarily crude.

Seeing that the systematic changes in the light curve during the 10-day span of our observations were relatively small, with apparent shifts less than 0.01 mag at a given orbital phase, we calculated a mean light curve from the entire time series. This is presented in Figure 2.

2.3. DDO spectroscopy

We obtained ground based spectroscopy of V471 Tau which partially overlapped with the MOST photometric run during 7 – 19 December 2005 (see Table 1). A total of 37 spectra at a dispersion of 0.14 Å/pixel were collected using the Cassegrain spectrograph of the 1.88-m telescope at the David Dunlap Observatory. Since we expected the K-type dwarf in the system to dominate the flux at optical wavelengths, the wavelength range of the spectra was centered at $H\alpha$ line, covering a red spectral window between 6425 and 6705 Å, (Figure 3). This region contains a multitude of telluric lines which were removed during standard reductions performed using IRAF² routines. The spectra were taken with the integration times and at intervals of about 30 minutes and could not cover all orbital phases of the binary because of the night/day breaks, commensurability of the binary period with one day and interruptions due to weather. The long integration times preclude any use of the spectroscopic data for improvement of the eclipse timing described in Section 3.2.

3. INTERPRETING THE LIGHT CURVE

The phase diagram of the mean light curve presented in Figure 2 was modeled using the PHOEBE software package (Prša & Zwitter 2005), based on the Wilson-Devinney model. The orbital and physical parameters of both stars in the system were adopted from O’Brien et al. (2001): $R_K = 0.96 R_\odot$, $T_K = 5,040 K$, $R_{WD} = 0.0107 R_\odot$, $T_{WD} = 34,500 K$, $a = 3.30 R_\odot$, $i = 77.4^\circ$; the subscripts K and WD signify the K and white dwarf components, respectively. The atmospheric parameters for the red dwarf component were set to typical values for a K dwarf; limb darkening = 0.52, gravity darkening = 0.32 and albedo = 0.5.

The resulting model reproduces the general nature and amplitudes of the double-wave variability, and the depth of the eclipse, seen in the MOST light curve, as shown in Figure 2. It consists of the dominant smooth, wave-like variability and a relatively shallow (0.022-mag deep) total eclipse lasting 46.9 minutes, with steep shoulders each approximately 50 sec long. The photometric double wave is caused by ellipsoidal distortion of the K dwarf, with a minor modification due to the reflection effect. The asymmetry in the ellipsoidal distortion variability is believed to be due to spots on the K dwarf.

²IRAF is distributed by the National Optical Astronomy Observatories, which are operated by the Association of Universities for Research in Astronomy, Inc., under cooperative agreement with the National Science Foundation.

3.1. Spot coverage

In order to study the locations and extent of spots on the surface of the K dwarf, we used the residuals between the observed light curve and the modeled light curve (Figure 4) to estimate the required changes of the spot filling factor with orbital phase. Because of the orbital inclination of 77° , it is only possible to estimate changes in the mean spot coverage on the K dwarf disk within the latitude range of -77° to $+77^\circ$. Recent Doppler imaging observations of Hussain et al. (2006) revealed that the K dwarf is rotating rigidly; this is confirmed by our determination of $V_K \sin i$ (Section 4.2). As our run duration was only 2.5 times longer than the time span of the observation used by Hussain et al. (2006), we expect any changes of filling factor at a given phase to reflect spot rearrangement caused by the star activity rather than the star differential rotation. Also, any spot interpretation can address only the part of the spot coverage which is longitudinally asymmetric.

Our results indicate that the smallest spot coverage occurred during the orbital phases 0.6 – 0.7, while the largest occurred during 0.2 – 0.3. We seem to have observed a totally different level of activity in the K dwarf than seen during the Doppler imaging observations by Ramseyer et al. (1995) and Hussain et al. (2006). Our estimate of the peak-to-peak amplitude of the spot filling factor, 0.02 – 0.03 (depending on the assumed spot temperature differential values of $\Delta T = 2,000 - 1,000 K$, as shown in Figure 4), is many times smaller than the changes of ~ 0.15 observed by Hussain et al. (2006) in November 2002. Also, in our data, the maximum spot coverage is inferred close to orbital phase 0.25, while Hussain et al. (2006) found the maximum around phase 0.07. The *evolution* of the spot coverage during the 10-day MOST observing run was still smaller, typically at a level of ≤ 0.01 , depending on the phase.

3.2. Eclipse timing

The relatively slow 10-sec photometric sampling rate (compared with the eclipse branch duration of 50 sec) and the temporal gaps left after the data selection made it impossible to measure times of individual eclipses accurate to a few seconds. Instead, we calculated the average eclipse time on the basis of a phased light curve of the entire time series to compare with earlier eclipse times in the literature. The phases were computed with the linear ephemeris given by Guinan & Ribas (2001). Because previous eclipses have been observed over a long time span (~ 35 yr) and the orbital period of the binary is short, we adopted a uniform time system of Heliocentric Julian Date based on the Terrestrial Time (HJED), as advocated by Bastian (2000).

The eclipse time was determined after correction of the light curve for the local slope created by the photometric wave. Since all contacts of the eclipse are not well defined (see Figure 5) we determined the intersections of the averaged eclipse branches with horizontal line at the mid-depth level. The mid-point of both intersections corresponds to the mid-point of the eclipse. With the ephemeris of Guinan & Ribas (2001), our mean epoch corresponds to $E = 25,135$. The shift in the observed time of the mid-point of eclipse is large compared to the predicted zero phase by Guinan & Ribas (2001): $O - C = +248 \pm 7$ seconds, or over 4 minutes (see Figure 5). The MOST eclipse time determination is shown compared to all available published data (as discussed by Ibanoglu et al. (2005)) in Figure 6. The $O - C$ curve continues an upward trend seen for about the last 10,000 orbital cycles. The implications of the MOST timing point are explored below.

3.2.1. *Third body*

The V471 Tau period changes visible in the eclipse $O - C$ diagram have been interpreted previously by several others as a light-travel-time effect caused by a perturbing third star in a long-period orbit in the system (Ibanoglu et al. 1994; Guinan & Ribas 2001; Ibanoglu et al. 2005). This explanation is attractive because it could be reconciled with the main features of the $O - C$ diagram. It is also exciting because the mass of the hypothetical third body would be sub-stellar for a large range of possible inclination angles.

Our new eclipse timing measurement shows that the long-anticipated downward bend in the $O - C$ diagram has not yet happened. Moreover, it deviates substantially from the most recent third-body model proposed (Ibanoglu et al. 2005) by 52 sec, which is 3.6 times larger than σ of the residuals for this model, as shown in the lower panel of Figure 6. Indeed, the MOST point is the largest deviation from this model so far observed.

Therefore, we decided to recalculate the third-body model utilizing the same formalism as in Ibanoglu et al. (2005). With the new data augmented by the MOST result, the semi-amplitude of the $O - C$ variations, the third-body orbital period and its mass function are all slightly larger and longer than those given by Ibanoglu et al. (2005); see Table 2 for the full set of fitted parameters. The third-body orbital fit, although formally appropriate, remains uncertain because we still do not see the bend in the $O - C$ curve. In fact, as is shown in Subsection 3.2.3 below, it is reasonable to assume that the period has been constant since $E \approx 15,000$, i.e., over the last ~ 14 years. However, if we continue to see a straight line in future extensions of the $O - C$ diagram, this will not necessarily exclude the third-body hypothesis. Figure 6 includes a fit to a third-body model whose orbit has an even longer period which can still match the observations. Note that the orbital inclination

range necessary to preserve the sub-stellar mass of the third body will decrease to a very small range of angles if the current linear trend in the $O - C$ deviations continues.

The suggested parameters of the hypothetical third body in the V471 Tau system indicate that this object may be detectable with modern infrared telescopes or interferometers. With a larger mass function and a longer orbital period than in Guinan & Ribas (2001), the separation and brightness of the third body can be as large as 0.9 arc second and $K \sim 13.3$ mag; see Table 6 for predictions of the third body parameters for its different orbital inclinations.

3.2.2. *Apsidal motion*

If the binary orbit is even slightly ellipsoidal, it may show a motion of the line of apses. This explanation was mentioned by Herczeg (1975) and Skillman & Patterson (1988), but then dismissed as an unlikely cause for the changes in eclipse times. We performed a least-squares fit of the $O - C$ curve with the first-order formula given by Todoran (1972) and found that a very narrow range of eccentricity, $e = 0.0121 \pm 0.0006$ (with 98% confidence level), is required to explain the latest $O - C$ results we have presented. See Table 3 and Figure 7. Although the orbit is expected to circularize in a very close binary system like V471 Tau, our fit to a slightly non-zero eccentricity is surprisingly close to the one we find from our radial velocity orbital measurements (see Section 4.1 below).

3.2.3. *Sudden period changes*

Without assuming anything about the actual nature of the $O - C$ changes, it may be argued that the curve is composed of a few straight-line segments, each corresponding to a constant period, and of relatively short intervals where abrupt period changes take place. The portions of the $O - C$ diagram from epochs $E \approx 2,500$ to $10,500$ and from $E \approx 15,000$ onwards appear to be consistent with two different constant periods. Least-squares linear fits to both segments of the $O - C$ diagram yield periods of $0.52118305(4)$ and $0.52118384(4)$ days, respectively (the errors in parentheses are given in units of the last decimal place), corresponding to a relative period change of $\Delta P/P \simeq 1.5 \times 10^{-6}$.

A sudden period change may be explained as a result of mass transfer or mass loss in a binary. For V471 Tau, we do not know if the possible donor, the K dwarf, is more massive than the mass recipient, the WD, but this is the most probable (O’Brien et al. 2001). In that case, the favorable scenario of a recent period increase is mass loss at the

level of $\sim 3.8 \times 10^{-7} M_{\odot}/yr$ (Hilditch 2001). Taking the masses of both components at the limits of the O’Brien et al. (2001) ranges we can also consider the case when the donor is the less massive star. Such a situation would require conservative mass transfer at a level of $\sim 3.6 \times 10^{-6} M_{\odot}/yr$ to explain the recent period increase. Both mass-loss rates appear to be large and unlikely for V471 Tau as they would result in other detectable phenomena. Moreover, both a period increase and a period decrease have been observed for the system so the complete picture would have to be even more complex.

The latest period change took place over some $\Delta E \simeq 2500$ cycles so the inferred time scale, T , was $T = (d \ln P / dt)^{-1} \simeq 2 \times 10^6$ years. This is a relatively short time scale for any thermal equilibrium adjustment in the K dwarf, but of course may relate only to the outer layers of its envelope.

The standard deviation in the residuals of the second segment of $\sigma = 22.7$ s (Figure 7) is slightly larger than for any of the previous fits (14.9 s for the third-body model and 16.6 s for the apsidal motion model) but is still acceptable if superimposed upon possible short-timescale variations which are considered below.

3.2.4. *Periodic residuals from eclipse timing models*

Every one of the $O - C$ models we calculated generates residuals with σ larger than the accuracy of the eclipse timings (typically a few seconds). We performed a search for periodicities in the residuals and found that regardless of the model used, there is evidence for a 10-year period in the timing residuals.

To investigate this further, we decided to employ a multi-harmonic analysis of variance (MAOV) with 2 harmonics, as described in Schwarzenberg-Czerny (1996). This method uses orthogonal polynomials to model the data and the analysis of variance statistics to evaluate the quality of the result. The MAOV periodogram obeys Fisher’s probability distribution with $2N + 1$ and $K - 2N - 1$ degrees of freedom, where N is the number of harmonics used and K is the number of observations. The quantity $F(2N + 1, K - 2N - 1)$ shown in Figure 8 measures the ratio of powers of the periodic signal and residual, fully random noise.

The amplitude of the variations we find in the $O - C$ residuals is similar for all three models we adopted, at the level of 20–25 s and indeed indicates a typical underlying variation with a time scale of about 10 years. The 5.5-yr period found by Ibanoglu et al. (2005) – which was connected with the ~ 5 -yr period in the mean brightness variations of the system – is also present, but at a much lower significance level (see Figure 8).

3.3. Short-period oscillations

Fluctuations with a period of 555 s were discovered in soft X-ray flux from the V471 Tau system by the EXOSAT satellite (Jensen et al. 1986). In 1991, 131 hours of continuous U-band photometry of V471 Tau by the Whole Earth Telescope (WET) (Clemens et al. 1992) resulted in the detection of three periods: 554.63, 561.59 and 277.319 s. The dominant 555-s variability (with its 277s harmonic) was attributed directly to the accreting magnetic polar caps on the white dwarf component of the system, and the 562s signal to the same radiation reprocessed by the K dwarf atmosphere.

To search for short-period variations in the MOST photometry, we first removed variations caused by the binary revolution and rotation of the spotted component. The data were “rectified” by fitting the data with least-squares low-order polynomials and then dividing by the fitted function. The eclipses and flare events (see Section 3.4 below), accounting for about 7% of the total time series, were excluded from the fit, resulting in a net duty-cycle of 59%. The remaining 52,371 brightness measurements of the binary, as well as corresponding measurements of both reference stars, were used to calculate MAOV periodograms, as described above in Subsection 3.2.4.

Analysis of the resulting periodogram revealed that none of the three WET periods is present in the MOST data, but their absence is easy to understand. While the white dwarf contribution to the total brightness of the system in the U band is about 39%, it is only 2.3% in the broad MOST photometric bandpass which includes considerable red flux. Therefore, the relative amplitude of the variations in MOST photometry is expected to be about 17 times smaller than in WET photometry. The relative signal would be $\sim 1.8 \times 10^{-4}$, which is slightly below our estimated, one-sigma detection limit of about 2×10^{-4} in these data. This value was calculated by folding the data with a period incommensurate with any of the V471 Tau variations and MOST orbital harmonics. The noise estimation was also confirmed with the photometric data of both reference stars.

Thus, the non-detection of the white dwarf pulsations in the broad MOST passband is entirely predictable. We can conclude only that the pulse amplitude (and presumably the polar accretion rate) did not increase significantly since the WET campaign in 1991.

3.4. Flare activity

Several flare-like events have been reported in V471 Tau by Rucinski (1981), Tunca et al. (1993), Ibanoglu et al. (2005) and others. Young et al. (1983) found that flares are most likely to occur when the brightness of the system is near its minimum, when the K dwarf

was thought to have its most spotted hemisphere facing Earth.

In the MOST light curve, we identified seven events we would consider flare-like, although two of them were only partially recorded due to gaps in the data. This is the first detection of white-light flares by the MOST satellite and probably the largest homogeneous set of V471 Tau flare-like events observed so far. The durations of these events varied from about 10 to over 35 minutes, but their shapes all share the same rapid rise and slower decay characteristic of flares seen in visible light. The candidate events are shown in Figure 9.

In contrast to Young et al. (1983), we did not find any correlation of the flare events with the photometric wave minimum. The flares occurred during phases of the lowest as well as the highest spottedness of the K dwarf, with no apparent concentration in phase. The symbols at the bottom of Figure 4 mark the phases when the flares occurred. Using luminosities of both components in the V band given by O’Brien et al. (2001), we estimated a lower limit to the energy released during the whole duration of a typical flare observed during the MOST run at about 10^{34} erg (see Table 4). The energies of each of the seven flares we observed are comparable to the energy released by the flare reported by Ibanoglu et al. (2005) and are at the top of the range of energies released by all flare-like events reported for V471 Tau. Because the activity cycle of V471 Tau still remains to be characterized in terms of its period and intensity, we cannot relate the observed incidence of flares to the phase in this cycle. We note only that all the observed flares share the shape, duration and energy with those reported for typical RS CVn systems.

The number of detected flare-like events corresponds to a total number of about 10 such events during the 10-day span of the MOST observations. Considering the limitations of ground-based observations one would expect to be able to detect a maximum of 4 flare-like events during the same period of time.

4. INTERPRETING THE SPECTRA

The typical S/N of the DDO spectra of V471 Tau is about 30. The contribution of the white dwarf component to the total light in the observed wavelength range is less than 1%, so its contributions to the spectroscopic analyses described below are negligible. Our discussion of the spectroscopic results is limited to the K dwarf in the system.

4.1. Radial velocities

To derive the radial velocities (RV) of the K dwarf, we used the Broadening Function (BF) technique (Rucinski 1999). Spectra of four different K-type standard stars (HD 62509, HD 65583, HD 3765, HD 103095) were adopted as templates. The resulting broadening functions were fitted by a rotational line-broadening profile, with a linear limb-darkening coefficient of 0.52 (assumed to be typical for a K-type dwarf in the observed wavelength range), following van Hamme (1993). The resulting RV measurements are listed in Table 1.

We performed two independent least-squares fits to the radial velocities, assuming first a circular and then an eccentric orbit, at a fixed orbital period as given by Guinan & Ribas (2001), but with the time of conjunction taken from the MOST light curve. The results of the fits and their residuals are plotted in Figure 10. The quality of both fits, evaluated by calculating the standard deviations of the residuals, is essentially identical for both types of orbits, with $\sigma \simeq 1.25 \text{ km s}^{-1}$. The fact that σ is not reduced for a model with more free parameters suggests that the eccentric orbit solution is not necessary (Lucy & Sweeney 1971), although obviously this is not a proof for perfect circularity of the V471 Tau orbit.

All our orbital model parameters (Table 5) agree very well with those obtained recently by Hussain et al. (2006), but they deviate slightly from those obtained previously with the same DDO 1.88-m telescope by Bois et al. (1988). The amplitude we find is larger by about $1.5 - 2 \text{ km s}^{-1}$, and the center-of-mass radial velocity is about 2 km s^{-1} smaller.

4.2. Projected rotation velocity

A bonus of the BF analysis is the availability of the projected rotation profile of the star onto radial velocity space (Figure 11). This shape can be interpreted through a solid-body rotation to estimate the projected equatorial velocity $V_K \sin i$. In the BF determination, we used HD 3765 as a standard star because its spectral type, K2V, is identical to that of the V471 Tau K dwarf. An average of the projected rotational velocities for all spectra is $V_K \sin i = 91.9 \pm 2.5 \text{ km s}^{-1}$. The value is corrected for the broadening introduced by the method, the magnitude of which can be estimated by applying the BF method to the template itself. The result is consistent with previous estimates made by Ramseyer et al. (1995) and Hussain et al. (2006) (91 ± 4 and $91 \pm 2 \text{ km s}^{-1}$, respectively) and all are consistent with synchronous rotation of the K dwarf in V471 Tau.

4.3. $H\alpha$ emission

The $H\alpha$ line was detected in emission in V471 Tau by Lanning & Etzel (1976). Subsequent detailed studies (Young et al. 1988; Bois et al. 1991; Rottler et al. 2002) revealed orbital phase-dependence of the emission as well as long-term changes of its equivalent width.

We extracted the $H\alpha$ emission from the absorption profiles of our spectra by again using the standard star HD 3765 as a template. HD 3765 has the same spectral type as the V471 Tau K dwarf and rotates very slowly at $V \sin i \simeq 1 \text{ km s}^{-1}$ (Soderblom 1985). We convolved the standard spectrum with the rotational profile calculated for $V_K \sin i = 92 \text{ km s}^{-1}$ (our value for V471 Tau) and fitted the resulting modified spectrum to each of our V471 Tau spectra in two wavelength ranges: $6540 - 6555 \text{ \AA}$ and $6570 - 6585 \text{ \AA}$ (see Figures 3 and 12). Subsequently, we used the net $H\alpha$ emission to derive the radial velocities and equivalent widths of the emission line (Table 1). The extracted $H\alpha$ profiles were symmetrical thus allowing us to use a Gaussian fit for measuring RV and numerical integration for equivalent widths. The radial velocity of the $H\alpha$ emission (Figure 13) follows the K dwarf orbital variations, but with a smaller amplitude of about 120 km s^{-1} , as estimated from a sinusoidal fit. Such behavior was observed during 1975 – 1984 by Bois et al. (1991), but with a still much smaller amplitude of $\sim 75 \text{ km s}^{-1}$. We observe that the $H\alpha$ equivalent width changes symmetrically with respect to its maximum at orbital phase 0.5 (Figure 13), in a very similar way to what was reported by Bois et al. (1991). The amplitude of the equivalent width variability in our data is about 1.2 \AA with the maximum emission of about -0.5 \AA at phase 0.5.

Long-term changes of $H\alpha$ emission were detected by Bois et al. (1991), who showed that the emission strength diminished between 1975 and 1983 and then grew rapidly in 1984. More recent observations by Rottler et al. (2002) have shown that since 1985, the emission was dropping again, until it finally vanished in 1992. This suggests that the long-term variation in $H\alpha$ emission strength may be periodic, with a period of roughly 9 years. Our measurements show that in December 2005, the emission strength was comparable to its average values in the past. This is consistent with a 9-year periodicity, since our DDO spectra were obtained about 2 years after the latest expected emission maximum in such a cycle.

5. SUMMARY

The nearly continuous MOST spacebased photometry of V471 Tau covering 10 days in December 2005, combined with partly simultaneous DDO groundbased spectroscopy, moni-

tored a fairly quiescent stage in the activity of the K dwarf in this close binary system. This is apparent in the light curve which deviates relatively little from the model and almost does not change during the whole observing run. Even during such a stable time, seven candidate flare events were observed in 10 days, whose estimated energies would be among the highest ever seen in V471 Tau. There is no correlation between the times of the flares and orbital phase.

The main features of the orbital phase diagram of the MOST photometry are well reproduced by our eclipsing binary light curve synthesis model. The largest systematic deviation in the double-wave light curve is only about 0.02 – 0.03 mag and is consistent with spots on the K dwarf which is expected to rotate synchronously with the orbit. The amount of spottedness on the star did not change much during the MOST observing run – by no more than about 1%. This supports the claim that the K dwarf was observed close to a minimum in its activity cycle. A half-orbital-period modulation of the radial velocity residuals was reported earlier by Hussain et al. (2006) and interpreted as an asymmetry in spot distribution on the K star’s surface. We see no such residuals in our radial velocity measurements. We note that the residuals seen by Hussain et al. (2006), the radial velocity curve we obtain, and the $O - C$ variations in eclipse times observed over the past 35 years, could all be interpreted as a small non-zero eccentricity of the orbit of V471 Tau.

Because of the broad bandpass of the MOST photometry with substantial flux in the red, and the red wavelength range of the DDO spectra, the white dwarf contributes only about 2% and 1% of the total intensity of the system, respectively. We were therefore unable to constrain the properties of the hot white dwarf in the system or confirm the oscillation frequencies detected by WET (Clemens et al. 1992), since the relative amplitudes in the custom-filter, broadband MOST photometry would be about 17 times smaller than in the WET U -band photometry. The positive aspect of this is that our estimates of the K dwarf properties from MOST photometry and DDO spectroscopy are not contaminated by the white dwarf, but we can use the timing of the white dwarf eclipses to investigate aspects of the orbit of the V471 Tau system.

Changes in the $O - C$ values of the times of eclipse of the white dwarf can, however, be explained by at least three entirely different models: (1) There could have been at least two abrupt period changes in the orbit of the system in the last 35 years, although there is no obvious mechanism for this. (2) There could be apsidal motion due to a slightly eccentric orbit. (3) The V471 Tau system might be a trinary, with a third low-mass companion in a long-period orbit. The last two periodic phenomena both predict that the $O - C$ eclipse timing deviations must drop in the future (see Figure 7). The small eccentricity which could explain the $O - C$ diagram is also in agreement with the formal solution of the radial velocity

curve of the K dwarf from our high-quality DDO spectra, but its value is currently below the direct spectroscopic detection threshold. Future accurate eclipse timing observations, such as performed by the MOST satellite, are desired as they may resolve the dilemma between those three models.

The $O - C$ residuals do show a convincing residual periodic variation with a period of about 10 years, regardless of the model used to explain the longer-term changes. This variation may be due to an activity cycle in the K dwarf, but this is a highly speculative explanation. We note that the $H\alpha$ emission appears to change in intensity in a characteristic time scale of about 9 years, perhaps coincident with the periodicity in eclipse time variations at the frequency resolution of the entire data sample at hand. The 10-year period in the $O - C$ residuals may also be related with the 5.5-year period in the system mean brightness variations found by Ibanoglu et al. (2005) as its multiple. Nevertheless we think that both periods are too uncertain to firmly connect them at this stage of the study of V471 Tau.

The DDO spectra yield a new radial velocity curve for the orbit of the K dwarf, and an improved determination of the projected rotation of the star, $V \sin i = 92 \text{ km s}^{-1}$ based on high-quality BF (broadening function) profiles. The spectra also enabled us to measure the $H\alpha$ emission velocities and changes in its equivalent width. The $H\alpha$ emission of V471 Tau showed the same orbital phase dependence as observed before by Bois et al. (1991) and Rottler et al. (2002) with maximum emission at phase ~ 0.5 . The observed amplitude of equivalent width variations of about 1.2 \AA was average for the system and consistent with the 9-year period noted by previous investigators. Unfortunately, the 13-year gap between the most recent published $H\alpha$ emission observations of V471 Tau and our new DDO observations does not allow us to reliably verify the periodic character of the mean emission strength variation.

A new feature of the $H\alpha$ emission revealed by our observations was its much larger amplitude of radial velocity variation (120 km s^{-1}) compared to that reported by earlier observers (75 km s^{-1} by Bois et al. (1991)). This suggests that the source of the emission was less concentrated around the sub-white-dwarf point on the K star as had been seen in the previous data.

The research of SMR, JMM, DBG, AFJM, DS and GAHW was supported by grants from NSERC (Natural Sciences and Engineering Council) Canada. WWW is supported by the Aeronautics and Space Agency of FFG and the Austrian Science Fund (FWF) P17580. RK is supported by the Canadian Space Agency through a contract with UBC. AFJM is supported from FQRNT (Quebec). KK appreciates the hospitality and support of the local staff during his stay at DDO. Special thanks are due to the DDO Telescope Operators,

Heide DeBond and Jim Thomson, for help with the spectroscopic observations, and to MOST Satellite Operators, Alex Beattie, Jamie Wells and Ron Wessels.

REFERENCES

- Bastian, U. 2000, *Inf. Bull. Var. Stars*, 4822
- Bois, B., Lanning, H. H., Mochnacki, S. W. 1988, *AJ*, 96, 157
- Bois, B., Lanning, H. H., Mochnacki, S. W. 1991, *AJ*, 102, 6
- Chabrier, G., Baraffe, I., Allard, F., Hauschildt, P. 2000, *ApJ*, 542, 464
- Clemens, J. C., Nather, R. E., Winget, D. E., Robinson, E. L., Wood, M. A., Claver, C. F., Provencal, J., Kleinman, S. J., Bradley, P. A., Frueh, M. L., Grauer, A. D., Hine, B. P., Fontaine, G., Achilleos, N., Wickramasinghe, D. T., Marar, T. M. K., Seetha, S., Ashoka, B. N., O’Donoghue, D., Warner, B., Kurtz, D. W., Martinez, P., Vauclair, G., Chevreton, M., Barstow, M. A., Kanaan, A., Kepler, S. O., Augusteijn, T., van Paradijs, J., Hansen, C. J. 1992, *ApJ*, 391, 773
- Guinan, E. F., Ribas, I. 2001, *ApJ*, 546, L43
- Herczeg, T. J. 1975, *Inf. Bull. Var. Stars*, No. 1076
- Hilditch, R. W. 2001, “An Introduction to Close Binary Stars”, Cambridge University Press, Cambridge
- Hussain, G. A. J., Allende Prieto, C., Saar, S. H., Still, M. 2006, *MNRAS*, 367, 1699
- Ibanoglu, C. 1978, *Ap&SS*, 57, 219
- Ibanoglu, C. 1989, *Ap&SS*, 161, 221
- Ibanoglu, C., Keskin, V., Akan, M. C., Evren, S., Tunca, Z. 1994, *A&A*, 281, 811
- Ibanoglu, C., Evren, S., Tas, G., Cakirli, O. 2005, *MNRAS*, 360, 1077
- Jensen, K. A., Swank, J. H., Petre, R., Guinan, E. F., Sion, E. M., Shipman, H. L. 1986, *ApJ*, 309, L27
- Lanning, H. H., Etzel, P. B. 1976, *Inf. Bull. Var. Stars*, No. 1147
- Lucy, L. B., Sweeney, M. A. 1971, *AJ*, 76, 544

- Matthews, J. M., Kuschnig, R., Guenther, D. B., Walker, G. A. H., Moffat, A. F. J., Rucinski, S. M., Sasselov, D., Weiss, W. W. 2004, *Nature*, 430, 921
- Moffat, A. F. J., 1969, *A&A*, 3, 455
- O’Brien, M. S., Bond, H. E., Sion, E. M. 2001, *ApJ*, 563, 971
- Prša, A., Zwitter, T. 2005, *ApJ*, 628, 426
- Ramseyer, T. F., Hatzes, A. P., Jablonski, F. 1995, *AJ*, 110, 3
- Rowe, J. F., Matthews, J. M., Seager, S., Kuschnig, R., Guenther, D. B., Moffat, A. F. J., Rucinski, S. M., Sasselov, D., Walker, G. A. H., Weiss, W. W. 2006, *ApJ*, 646, 1241
- Rottler, L., Batalha, C., Young, A., Vogt, S. 2002, *A&A*, 392, 535
- Rucinski, S. M. 1981, *Acta Astron.*, 31, 37
- Rucinski, S. M. 1999, in *ASP Conf. Ser. 185, Precise Stellar Radial Velocities*, ed. J. B. Hearnshaw & C. D. Scarfe (San Francisco: ASP), 82
- Schwarzenberg-Czerny, A. 1996, *ApJ*, 406, 107
- Skillman, D. R., Patterson, J. 1988, *AJ*, 96, 976
- Soderblom, D. R. 1985, *AJ*, 90, 10
- Still, M., Hussain, G. 2003, *ApJ*, 597, 1059
- Todoran, I. 1972, *Ap&SS*, 15, 229
- Tunca, Z., Keskin, V., Evren, S., Ibanoglu, C., Akan, M. C. 1993, *Ap&SS*, 204, 297
- van Hamme, W. 1993, *AJ*, 106, 2096
- Walker, G., Matthews, J., Kuschnig, R., Johnson, R., Rucinski, S., Pazder, J., Burley, G., Walker, A., Skaret, K., Zee, R., Grocott, S., Carroll, K., Sinclair, P., Sturgeon, D., Harron, J. 2003, *PASP*, 115, 1023
- Werner, K., Rauch, T. 1997, *A&A*, 324, L25
- Young, A., Klimke, A., Africano, J. L., Quigley, R., Radick, R. R., Van Buren, D. 1983, *ApJ*, 267, 655
- Young, A., Skumanich, A., Paylor, V. 1988, *ApJ*, 334, 397

Table 1. Spectroscopic observations.

No.	<i>HJED</i> – 2, 453, 700	photometric phase	S/N	V_{rad} (km s ⁻¹)	$H\alpha$ EW (Å)	v_{rad} of $H\alpha$ net emission (km s ⁻¹)
1	17.58275	0.5162	30	16.8	-0.578	42
2	17.71561	0.7717	30	-113.2	0.183	-77
3	17.72632	0.7922	30	-108.3	0.249	-57
4	17.73841	0.8154	30	-101.1	0.361	-77
5	17.74935	0.8364	30	-91.2	0.407	-70
6	17.76196	0.8606	30	-78.8	0.493	-22
7	17.77283	0.8815	30	-66.3	0.620	-7
8	17.78482	0.9045	12	-50.3	0.801	-11
9	17.79554	0.9250	30	-31.3	0.727	-7
10	17.80788	0.9487	30	-12.4	0.789	36
11	17.81871	0.9695	8	12.2	0.745	15
12	17.83145	0.9939	8	31.0	0.538	57
13	18.48312	0.2443	20	184.8	0.165	167
14	18.49374	0.2647	30	184.2	0.103	186
15	18.50572	0.2877	30	183.2	0.025	168
16	18.51648	0.3083	30	176.1	-0.050	166
17	18.52928	0.3329	30	165.2	-0.143	159
18	18.54004	0.3535	30	157.4	-0.207	141
19	18.55221	0.3768	30	142.2	-0.278	147
20	18.56299	0.3975	30	127.6	-0.375	129
21	18.57489	0.4203	30	107.5	-0.411	110
22	18.58558	0.4409	30	91.8	-0.485	92
23	18.59955	0.4677	30	63.3	-0.535	81
24	18.61024	0.4882	30	44.4	-0.544	62
25	18.62229	0.5113	30	22.4	-0.485	42
26	18.63295	0.5318	30	4.8	-0.520	26
27	18.64494	0.5548	30	-16.4	-0.388	18
28	18.65570	0.5754	30	-34.7	-0.319	3
29	18.66658	0.5976	15	-52.8	-0.298	-22
30	18.67986	0.6218	30	-70.3	-0.135	-25
31	18.69057	0.6423	30	-84.7	-0.102	-63
32	18.70082	0.6635	30	-92.5	-0.121	-42
33	23.79578	0.4377	30	91.5	-0.393	100
34	23.80649	0.4583	30	75.0	-0.447	90
35	23.81862	0.4816	10	53.2	-0.394	61
36	23.82925	0.5020	10	32.9	-0.440	55
37	23.84138	0.5252	20	6.5	-0.403	35

Table 2. The best fit parameters for a third body model.

parameter	value
T_0 (HJED)	$2440610.06446 \pm 0.00008$
P_0 (d)	$0.521183449 \pm 0.000000008$
P_3 (yr)	33.7 ± 0.9
$a_{12} \sin(i_3)$ (AU)	0.32 ± 0.02
semiamplitude (sec)	159 ± 6
e	0.28 ± 0.09
ω_3 (degr)	79 ± 10
$f(M_3)$ (M_\odot)	$(2.9 \pm 0.3) \cdot 10^{-5}$

Note. — The errors were estimated using the bootstrap sampling method for the 98% confidence level; this is why they appear to be large when compared to other fits, for example by Ibanoglu et al. (2005).

Table 3. The best fit parameters for the orbital apsidal motion.

parameter	value
P (day)	38.884 ± 0.007
semiamplitude (sec)	173 ± 9
e	0.0121 ± 0.0006
ω_0 (degr)	174 ± 3
ω_1 (degr/day)	0.025348 ± 0.000005

Table 4. A list of flare-like events observed by MOST.

nr	start time (HJED)	phase	duration (min)	ΔI_{max}	E_{min} (erg)
1	2453709.164	0.379	19	0.014	$9.8 \cdot 10^{33}$
2	2453709.351	0.738	12	0.014	$3.2 \cdot 10^{33}$
3*	2453710.59	0.12	> 16	> 0.016	$> 1.8 \cdot 10^{34}$
4	2453711.345	0.564	13	0.011	$1.0 \cdot 10^{34}$
5	2453714.770	0.135	36	0.018	$2.9 \cdot 10^{34}$
6*	2453717.01	0.43	> 33	0.018	$> 4.4 \cdot 10^{34}$
7	2453718.156	0.632	10	0.017	$1.9 \cdot 10^{34}$

Note. — E_{min} designates the lower limit for total energy released in the V band. The flares marked with a star were observed only partially.

Table 5. Parameters of spectroscopic orbits.

parameter	circular orbit	eccentric orbit
K_K (km s ⁻¹)	150.5 ± 0.4	150.2 ± 0.5
$a \sin i$ (R_\odot)	1.550 ± 0.004	1.547 ± 0.005
e	–	0.012 ± 0.003
ω_1 (degr)	–	75 ± 18
V_0 (km s ⁻¹)	35.7 ± 0.3	35.2 ± 0.3
σ (km s ⁻¹)	1.25	1.25

Table 6. Parameters of hypothetical third body in the V471 Tau system.

i_3 (degr)	M_3 (M_\odot)	T_{eff} (K)	$\log L/L_\odot$	m_V	m_K	d_{max} (mas)	T_{max} (year)
85	0.045	1540	–4.3	29.6	15.4	420	2014.1
60	0.052	1730	–4.1	26.8	15.0	490	2015.0
45	0.064	2060	–3.8	24.0	14.4	610	2016.1
30	0.090	2660	–3.2	19.2	13.3	910	2019.0

Note. — The physical parameters of the third body are based on nongray dusty models of Chabrier et al. (2000), assuming the age of the system of 625 Myr and the distance of 46.8 pc. d_{max} designates maximum apparent separation between the V471 Tau binary and the third component. T_{max} is the time of the nearest maximum separation.

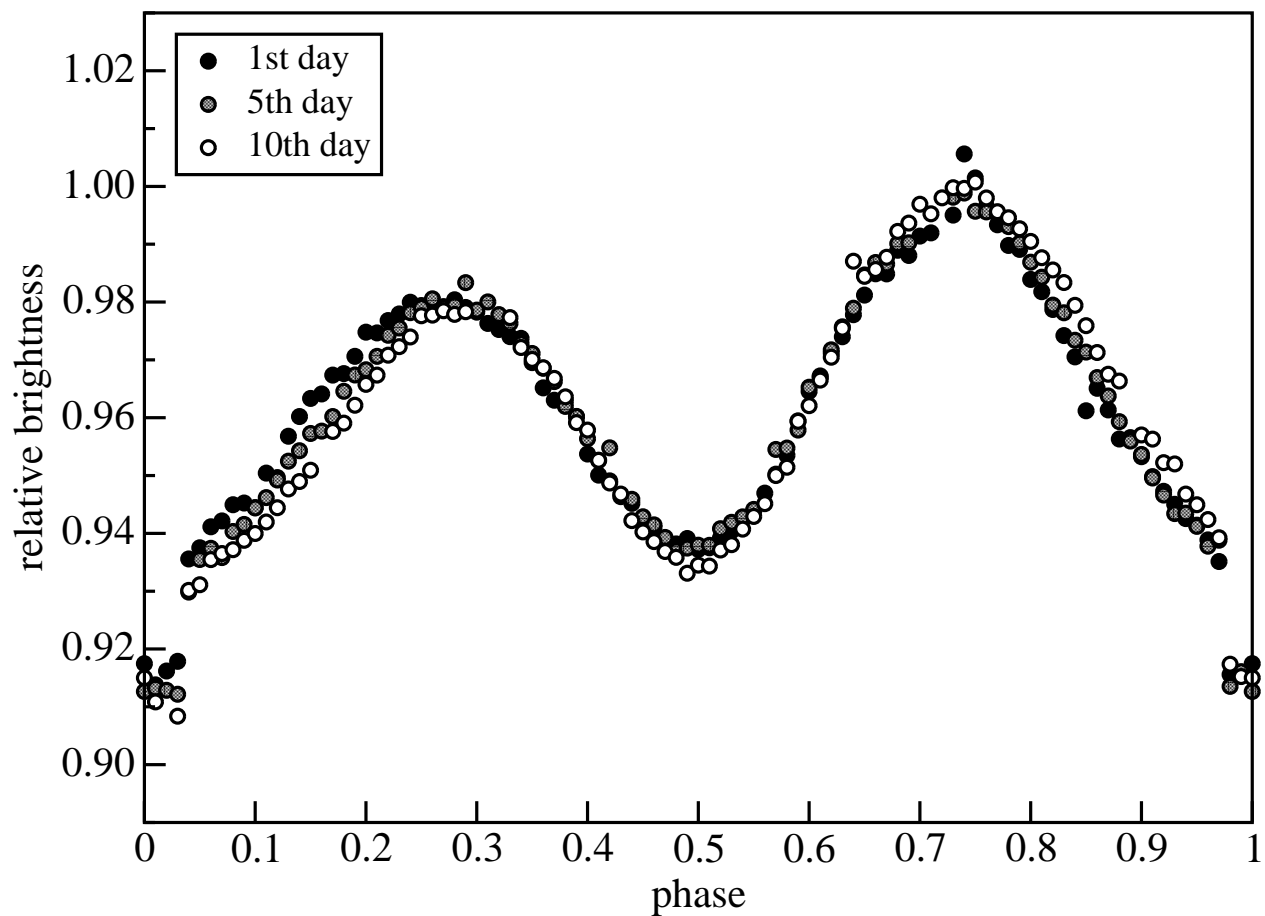


Fig. 1.— The mean V471 Tau light curve, averaged in phase with 0.01 phase bins, for 3 selected days of the MOST observations at the beginning, middle and end of the run. A lack of obvious changes in the light curve during our observations beyond the global shifting at phases $\sim 0.75 - 1.25$, can be interpreted as a relatively low activity in the spot re-arrangement.

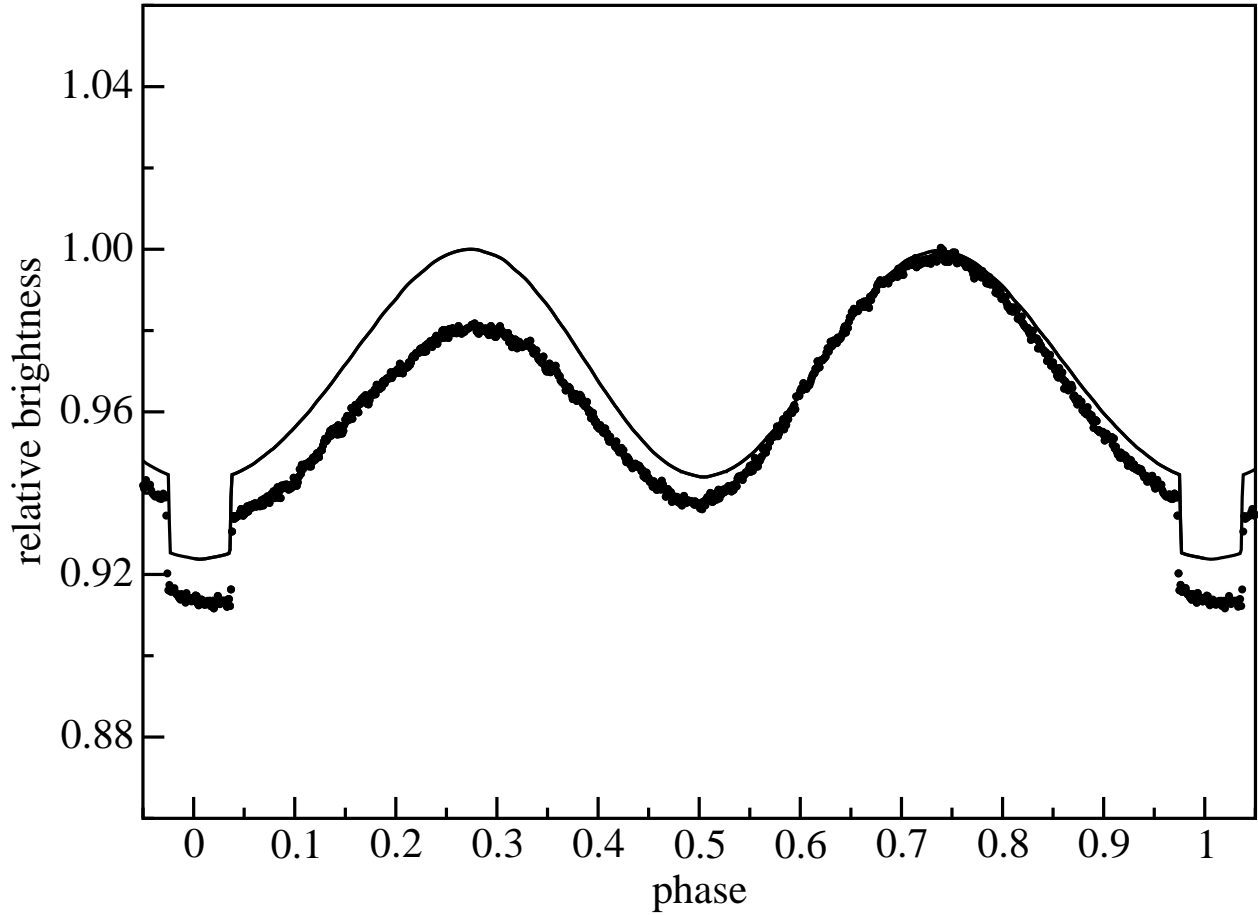


Fig. 2.— The mean V471 Tau light curve averaged in phase with 0.001 phase bins (dots). The line shows the light curve calculated by the PHOEBE package (Prša & Zwitter 2005), based on the published V471 Tau parameters. Deviations caused by the spots on the K dwarf are not included in the model.

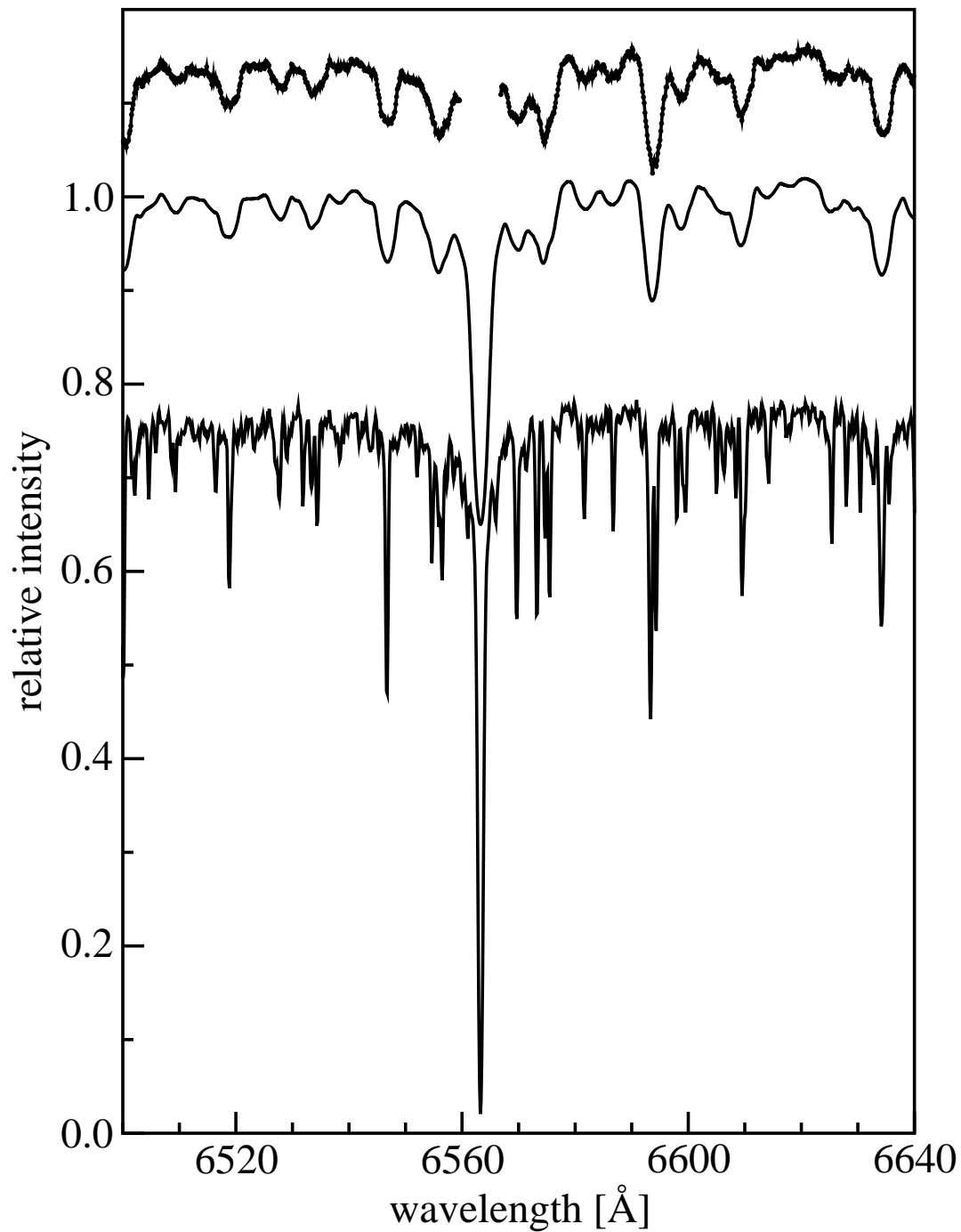


Fig. 3.— Comparison of the DDO spectra of V471 Tau. Top: The average of the 27 best quality spectra after correction shifts for the orbital motion. The $H\alpha$ line was omitted due to its variability (see Subsection 4.3) Middle: The standard star HD 3765 spectrum after convolution with the broadening profile. Bottom: The HD 3765 spectrum as observed.

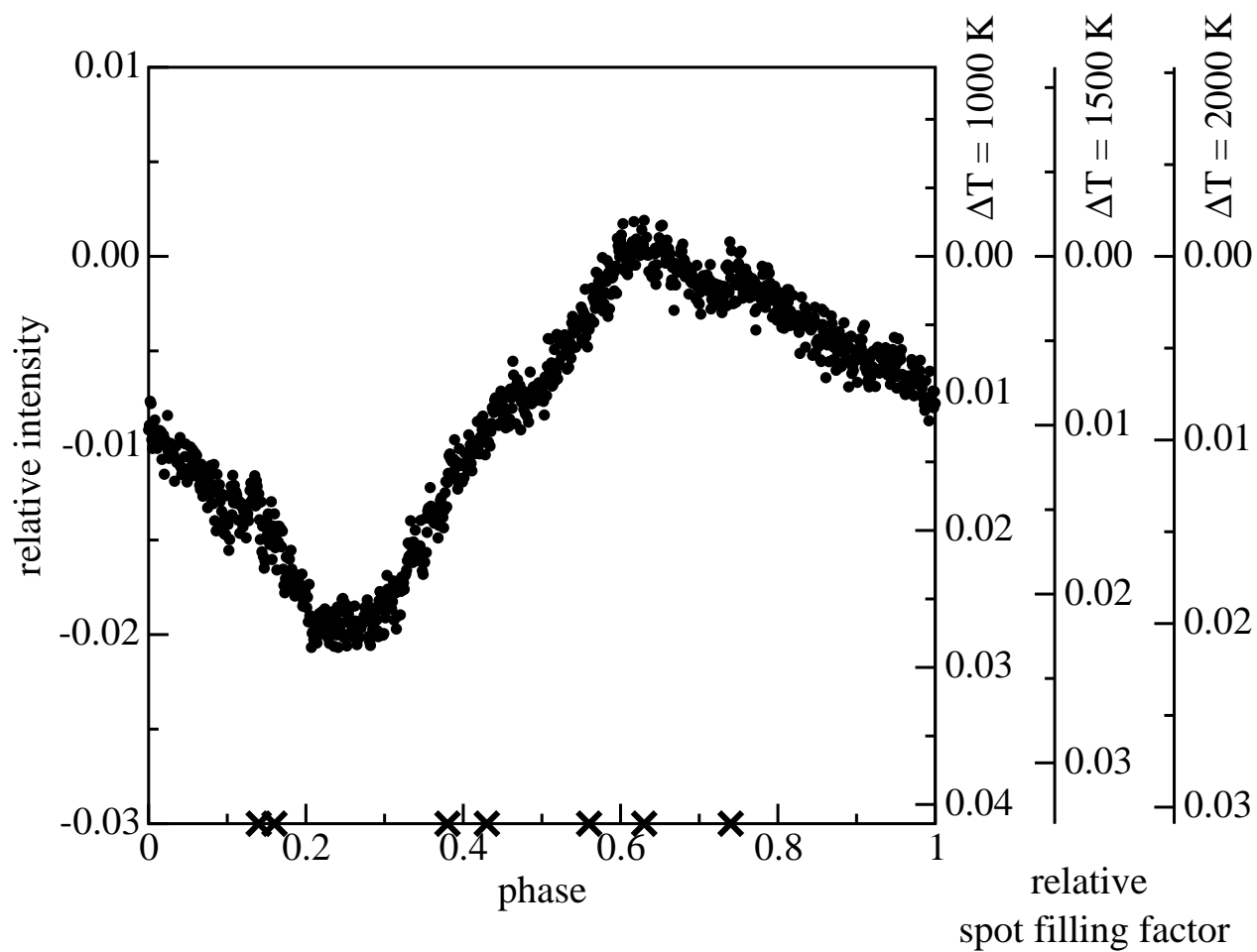


Fig. 4.— Relative changes of the spot-filling factor versus the orbital phase for different spot temperatures, as indicated on the right vertical axis. The curve was obtained by comparing observed light curve (averaged in phase with 0.001 phase bins) with the theoretical one calculated with the PHOEBE package, as described in the text. The crosses on the bottom axis mark the phases of seven detected flare-like events (see Subsection 3.4).

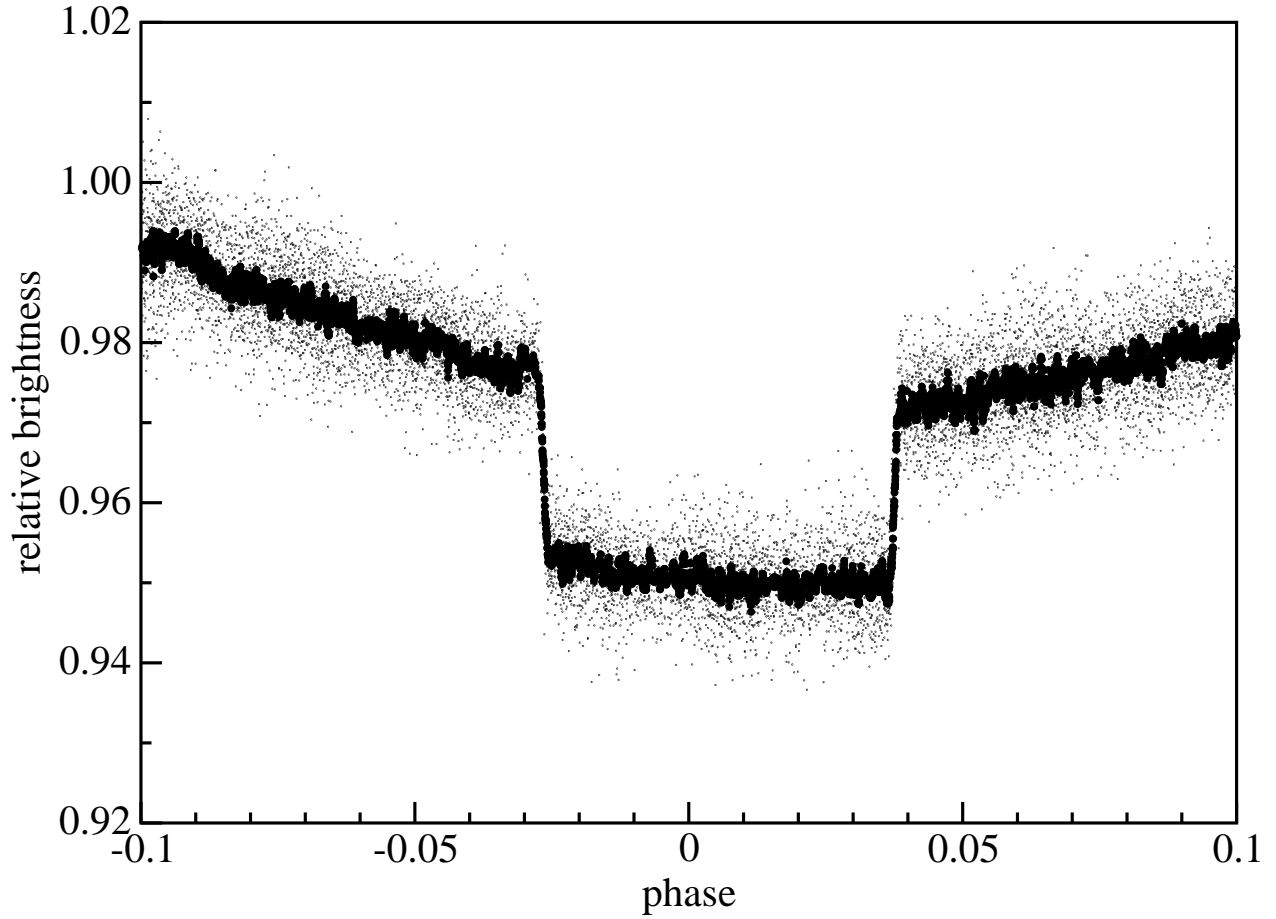


Fig. 5.— All observations used for the V471 Tau eclipse timing (small dots) are shown in the phase diagram together with the running average data (large dots). The phase shift of the mid-eclipse time relative to the Guinan & Ribas (2001) linear ephemeris is clearly visible.

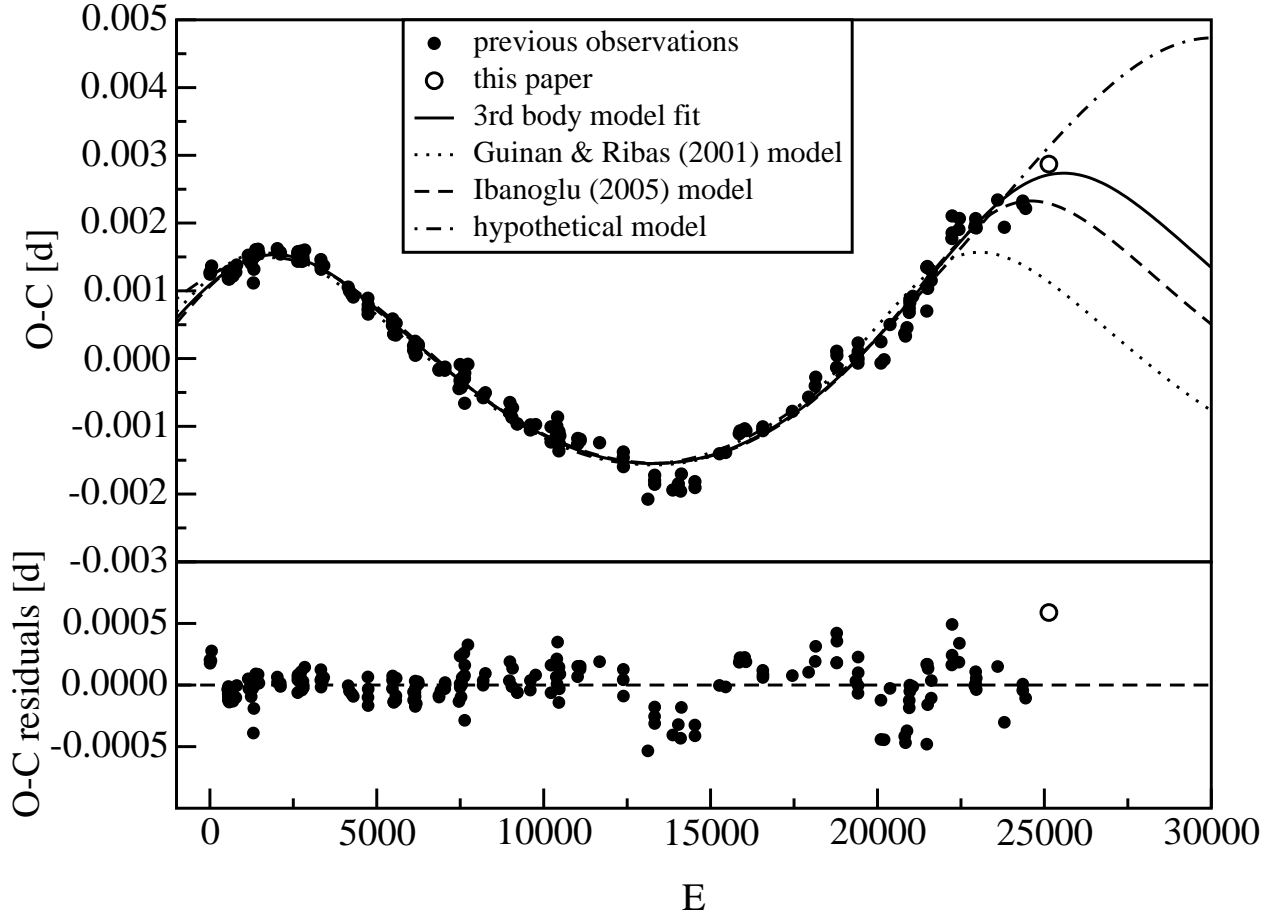


Fig. 6.— The third-body model fits to eclipse timing observations of V471 Tau from the literature (filled circles). The open circle is the new timing from the MOST observations. A hypothetical, illustrative trend was created by adding a point of $O - C = 0.004480$ at $E = 28,000$, that would follow the curve growing trend. The bottom plot shows the residuals of all available data with respect to the model predictions of Ibanoglu et al. (2005).

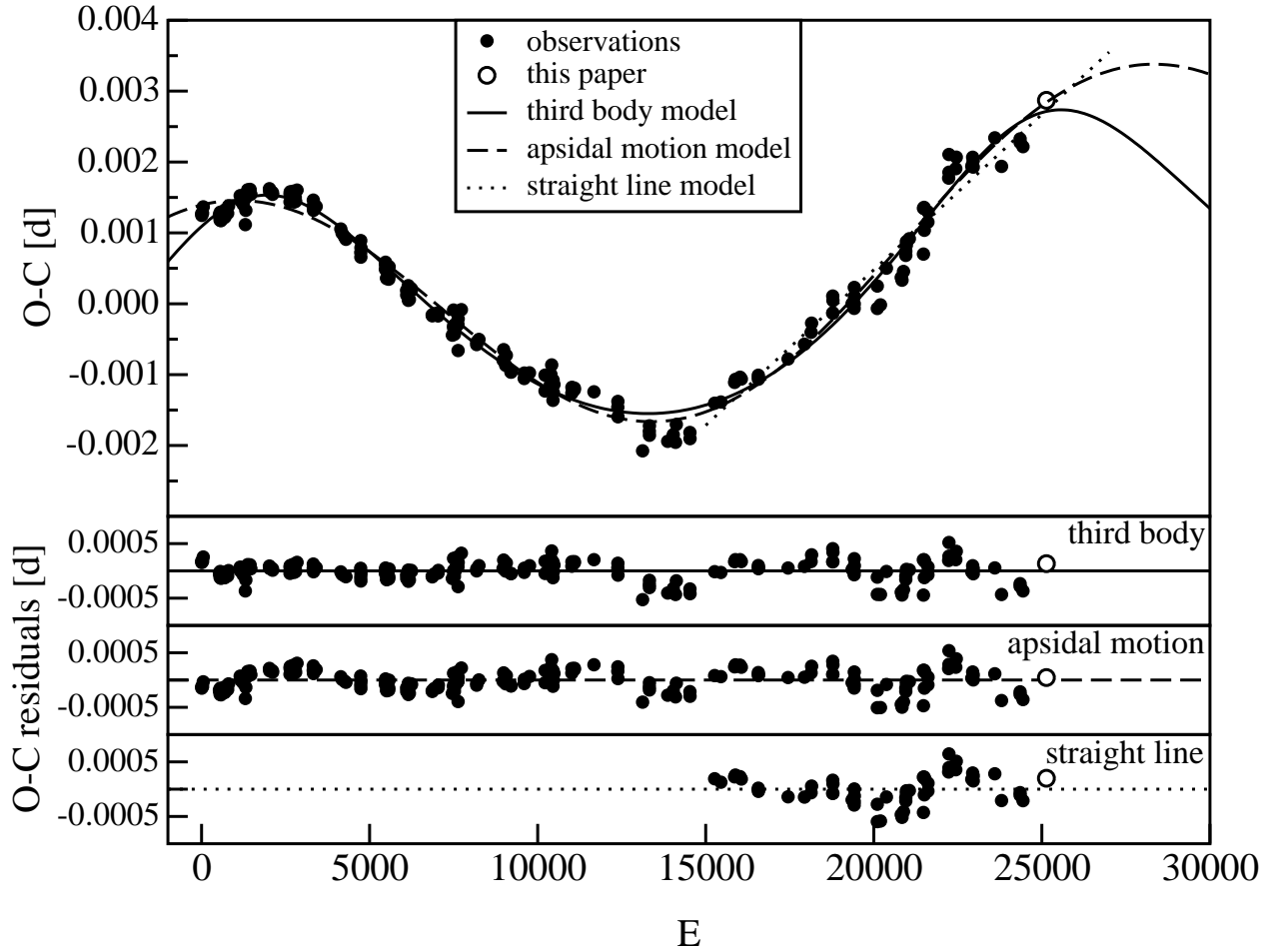


Fig. 7.— Comparison of the third body, apsidal motion and straight line model fits to the available eclipse time observations of V471 Tau.

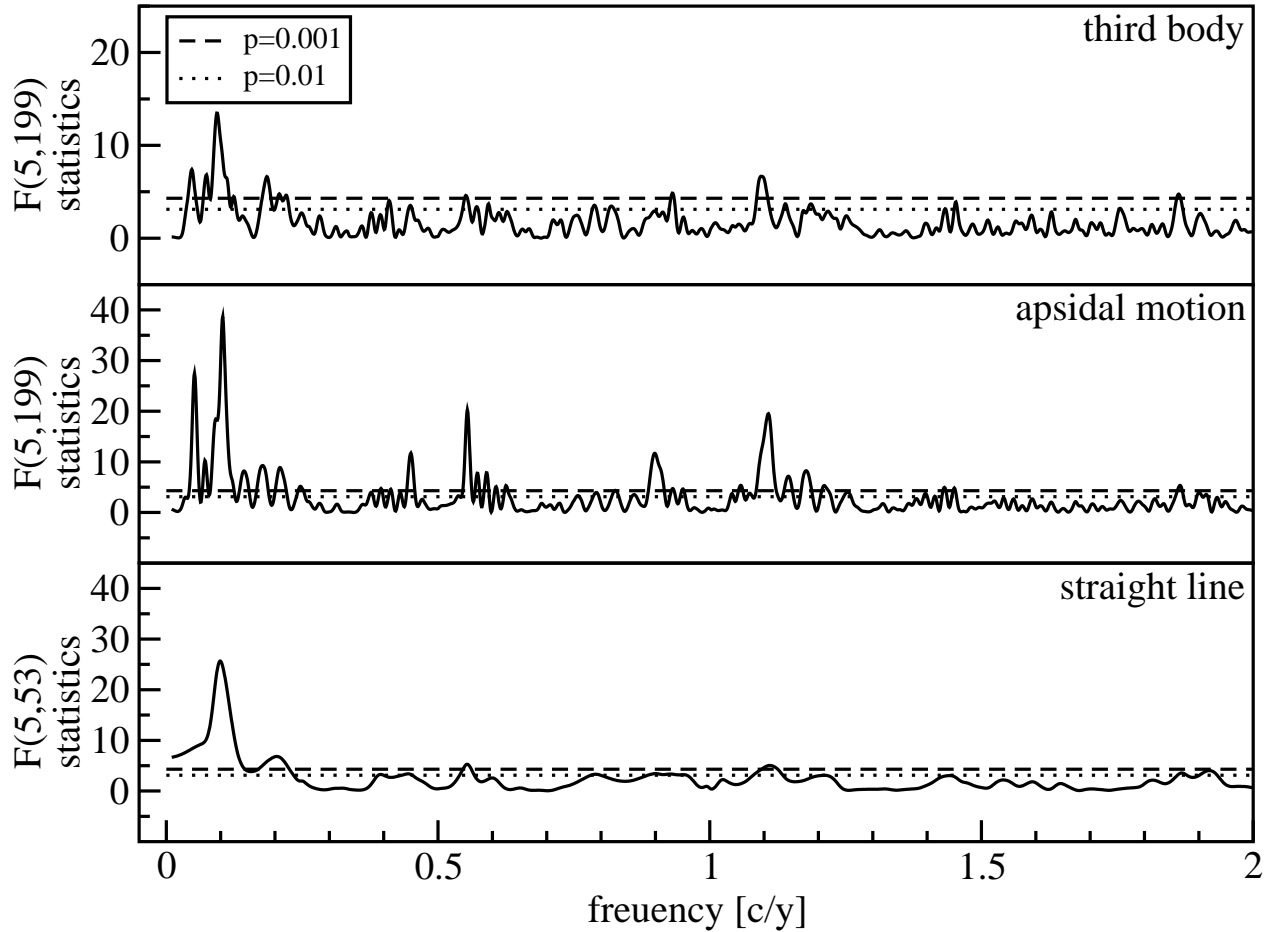


Fig. 8.— Multiharmonic analysis of variance periodograms (Schwarzenberg-Czerny 1996), with frequencies up to 2 cycles per year, for different model residuals, as discussed in Subsection 3.2. Horizontal lines show the levels of 0.001 (dashed line) and 0.01 (dotted line) probability of false detection. The most significant peaks appear around the same frequency ~ 0.1 c/y for all models (the top two periodograms also show its alias at ~ 0.05 c/y). Note that the 5.5 yr period (0.18 c/y) found by Ibanoglu et al. (2005) appears to be also present.

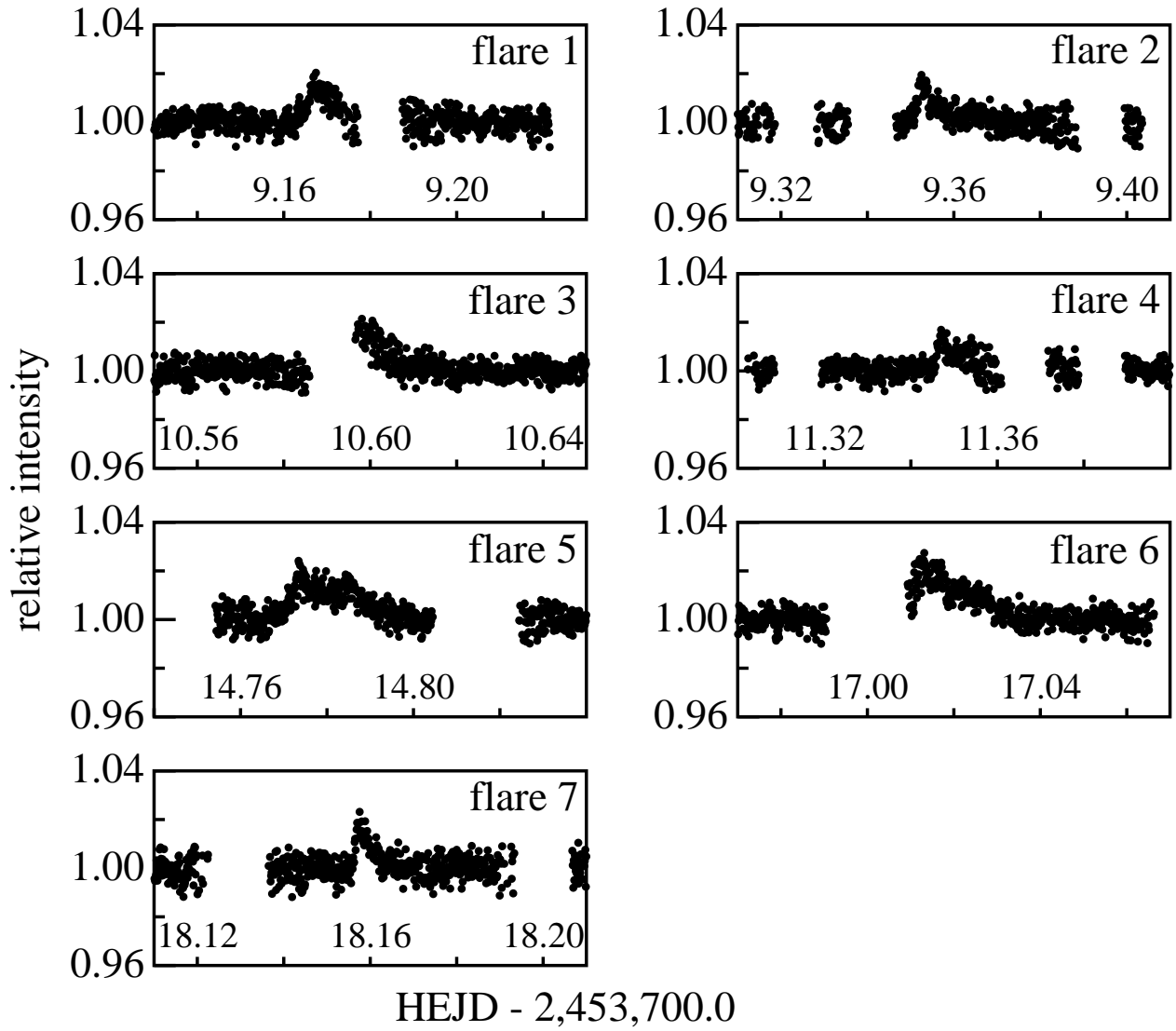


Fig. 9.— The seven flare-like events on V471 Tau which were detected during MOST observation period.

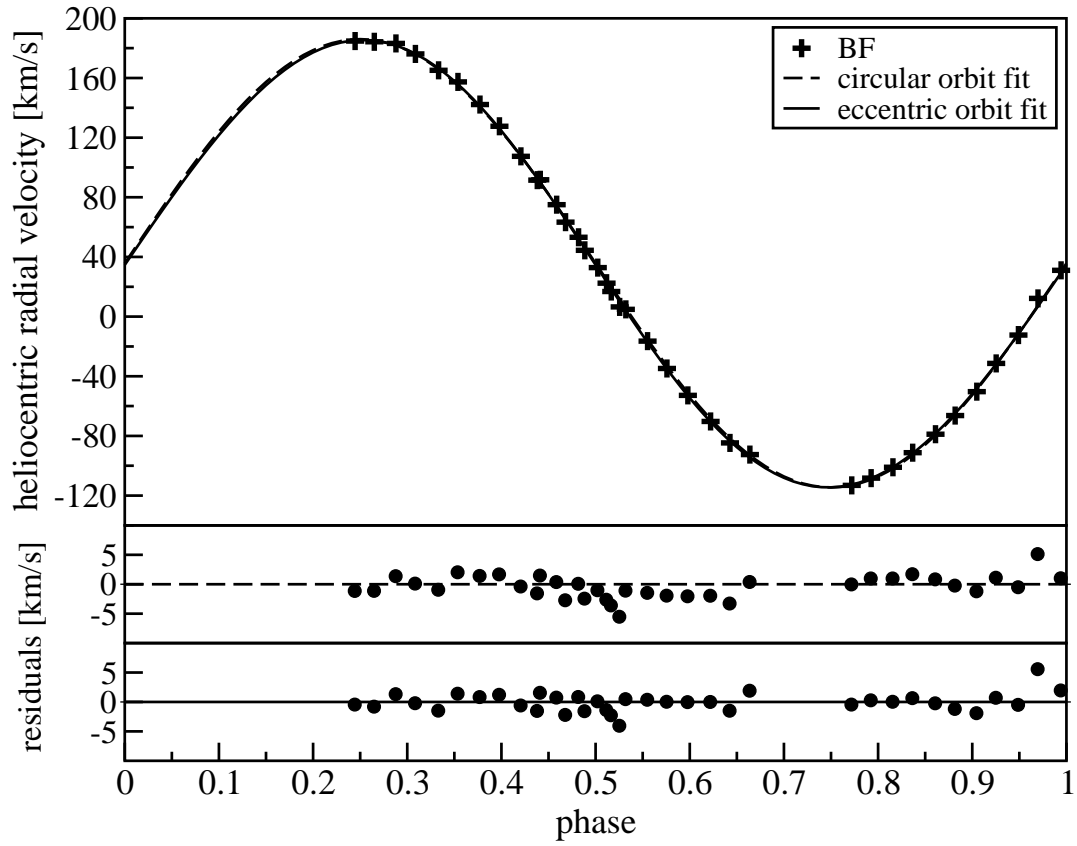


Fig. 10.— The radial velocity curve for the K dwarf component of V471 Tau binary. The bottom panels show residuals for the circular and elliptical models, respectively.

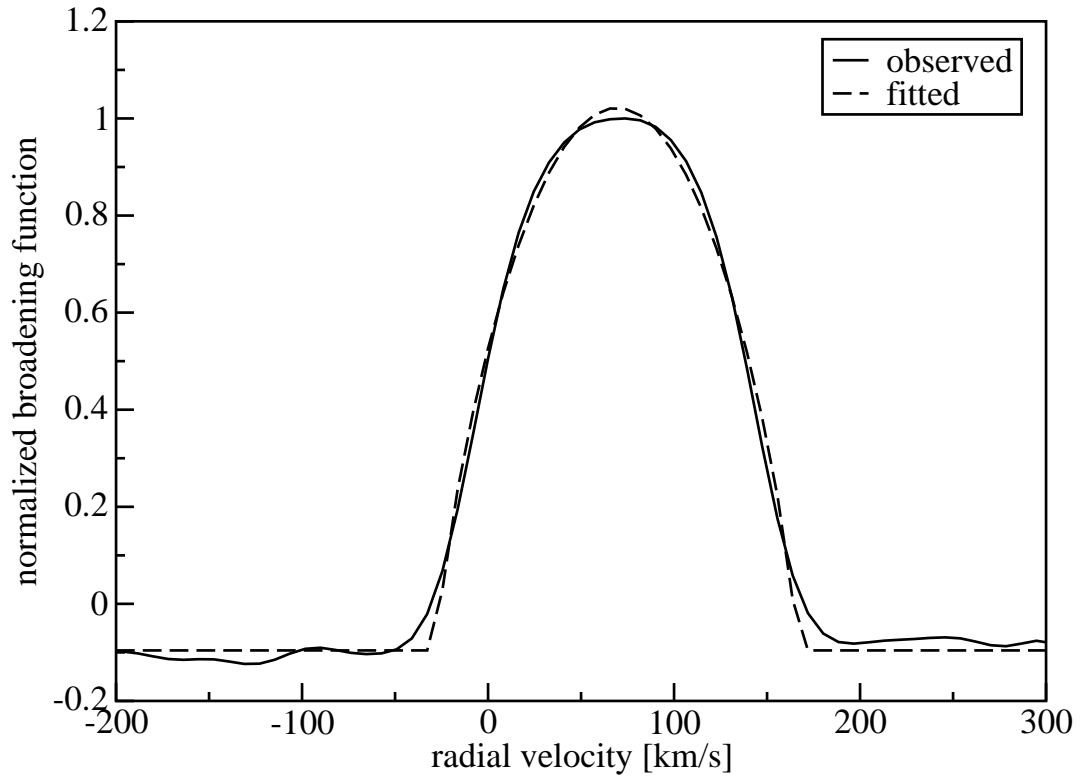


Fig. 11.— The average broadening function of V471 Tau spectra derived with the standard velocity star HD 3765 of the same spectral type (solid line). This BF profile was fitted by the rotational broadening profile to estimate the projected rotation velocity of the K dwarf component (dashed line).

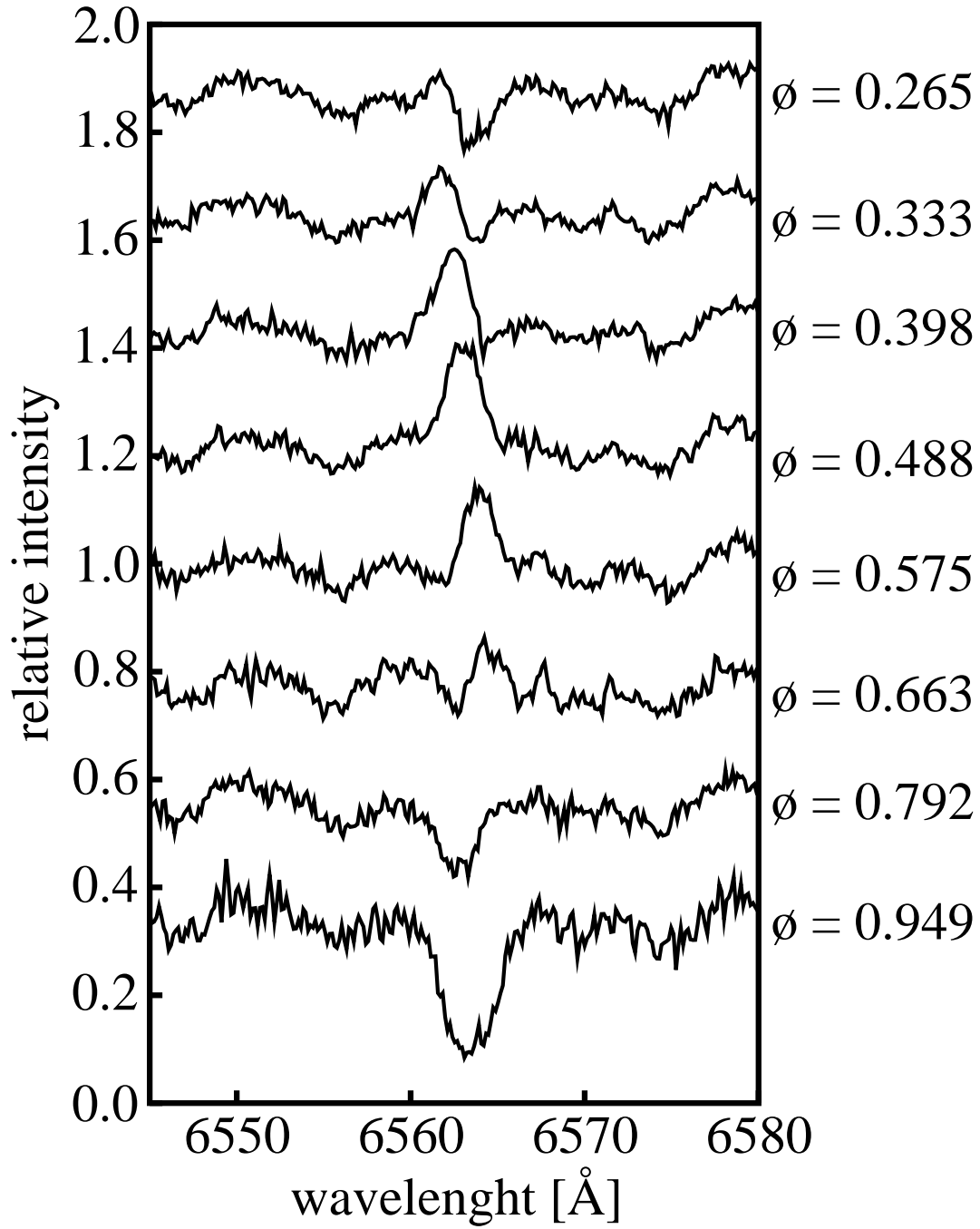


Fig. 12.— A collection of representative spectra of V471 Tau taken at different phases. The variable strength and shifts in position of the $H\alpha$ emission are clearly visible.

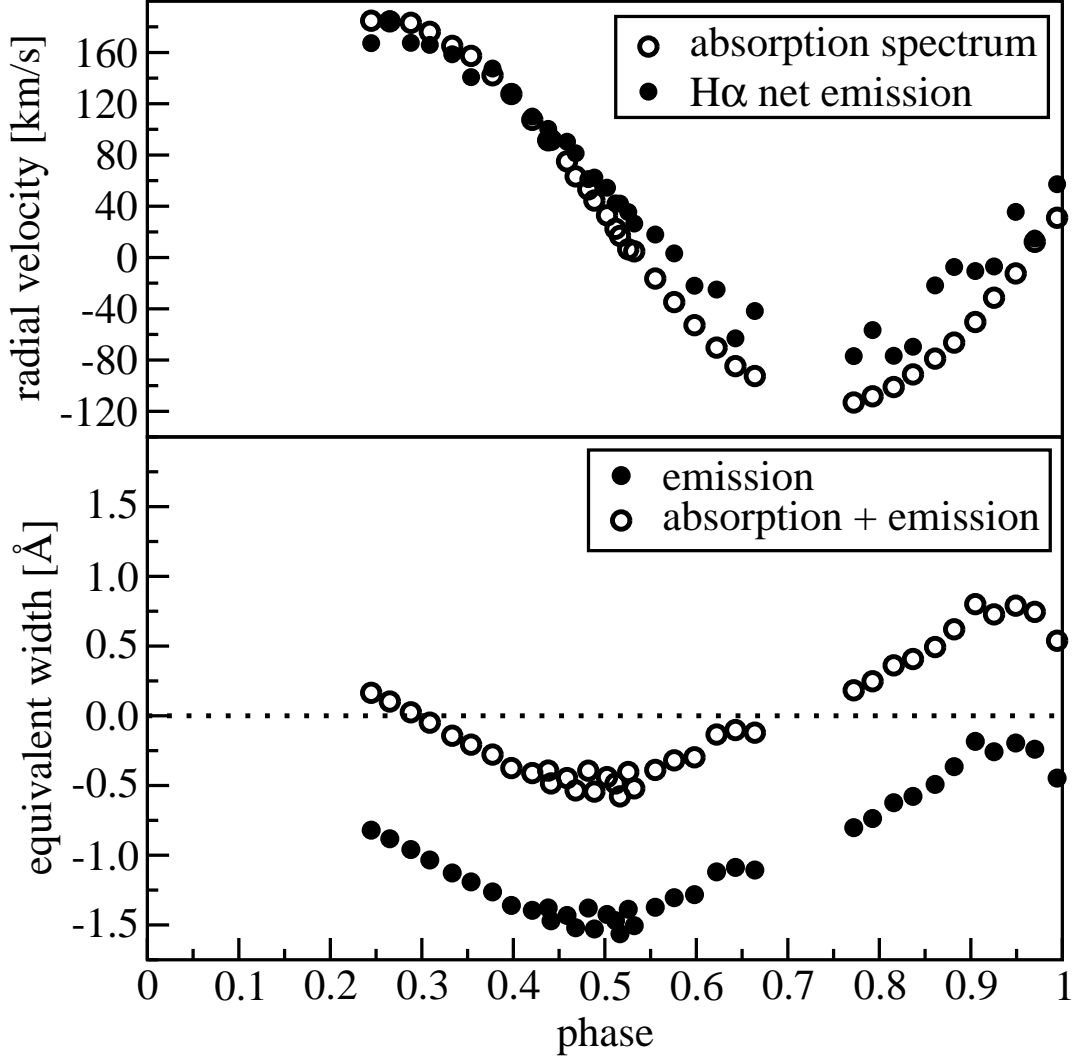


Fig. 13.— Variations of the $H\alpha$ emission line. Top: The radial velocity changes of the net emission with phase, compared with those of the K-dwarf itself (the absorption spectrum). Note the reduced amplitude of about 120 km s^{-1} . Bottom: Changes of the $H\alpha$ line equivalent width. The strongest emission is visible when the K-dwarf component is seen in the upper conjunction (when the face illuminated by the WD is directed to the observer around the orbital phase of 0.5). The emission is practically undetectable during the opposite phases.